Experimental and modeling study of fluid pressure-driven fractures in Darley Dale sandstone

Sergio Vinciguerra
Osservatorio Vesuviano, Istituto Nazionale di Geofisica e Vulcanologia, Naples, Italy

Philip G. Meredith
Mineral, Ice and Rock Physics Laboratory, Department of Earth Sciences, University College London, London, UK

Jim Hazzard
Lassonde Institute, University of Toronto, Toronto, Ontario, Canada

Received 3 February 2004; revised 3 April 2004; accepted 14 April 2004; published 12 May 2004.

[1] We report measurements of acoustic emissions (AE) generated during formation and growth of pressure driven fractures in cylindrical samples of Darley Dale sandstone that were co-axially pre-drilled in order to allow an internal pressure to be applied. A set of 3 to 6 fractures initiate at the wall of the internal bore at a fluid pressure around three times that of the confining pressure, but only 3 propagate to the outer wall of the sample. Time and spatial distributions of acoustic emissions show two distinct bursts of activity, associated with initiation and propagation, respectively. A Particle Flow Code (PFC) model has been used to reproduce the mechanics of fracture initiation and the time and spatial distributions of AE. In both the experiments and the model, we observe a distinct phase of accelerating AE activity preceding fracture formation. *INDEX TERMS:* 5102 Physical Properties of Rocks: Acoustic properties; 5104 Physical Properties of Rocks: Fracture and flow; 5112 Physical Properties of Rocks: Microstructure. **Citation:** Vinciguerra, S., P. G. Meredith, and J. Hazzard (2004), Experimental and modeling study of fluid pressure-driven fractures in Darley Dale sandstone, *Geophys. Res. Lett.*, *31*, L09609, doi:10.1029/2004GL019638.

1. Introduction

[2] Fundamental understanding of how fluid pressure-driven fractures progressively nucleate and propagate is crucial to understanding a range of crustal weakening processes. The injection of fluid into a porous or fractured rock mass at a sufficiently high rate results in the propagation of tensile (mode I) fractures, which extend in the plane normal to the minimum principal stress. Examples of fluid pressure-driven fractures have been extensively reported in many areas of earth science, from structural geology and volcanology to petroleum geology, seismology and hydrogeology. Pore fluid pressure pulsing is recognized as an important crustal process, leading to cyclic episodes of pressure driven fracturing and the creation of fluid flow pathways, even at high lithostatic pressure. This process has also been invoked to explain deep crustal seismic reflectors and detachments, and large-scale horizontal fluid migration in the crust. Episodic pore fluid pressure build-up and release in the crust can also explain the formation of hydrothermal ore deposits, mineralized veins, and even some aspects of the mechanics of large earthquakes [*Secor and Pollard*, 1975*; Nur and Walder*, 1992].

[3] One of the most common natural manifestations of fluid pressure-driven fracturing is the occurrence of dykes related to volcanic activity. These serve as major conduits for magma transfer from the mantle to the upper crust, and constitute a common expression of crustal extension. Over the last two decades, interest in dyke mechanics has steadily increased. A number of theoretical studies, focusing mainly on dyke emplacement, have defined the conditions under which the sheet mode of magma transport and crustal deformation is favorable [*Weertman*, 1971; *Pollard*, 1987]. The application of principles from fracture mechanics and fluid mechanics has led to increasingly sophisticated analytical models [*Pollard*, 1987; *Spence and Turcotte*, 1985; *Lister and Kerr*, 1991; *Rubin*, 1993]. However, although analytical models have greatly increased our understanding of fluid pressure-driven fracturing, such models invariably oversimplify certain aspects of the mechanics, and it is therefore crucial that theoretical advances are accompanied by experimental observations. Acoustic emission (AE) monitoring of the fracture process provides important complementary information about the micromechanics of crack growth, crack interaction and failure of rock under stress. There is considerable evidence to show clear correspondence between the spatial and temporal distributions of AE activity in laboratory fracture experiments and patterns of seismic activity from natural rupture episodes [e.g., *Meredith et al.*, 1990; *Lockner et al.*, 1991]. Brittle rock fracture can thus be regarded as analogous to earthquake rupture, since it is found to obey similar statistics for source dimensions over more than eight orders of magnitude, from sub-grain-sized cracks to crustal earthquakes [*Hanks*, 1992; *Zang et al.*, 1998]. Although we also recognize the importance of chemical and thermal effects in promoting time-dependent subcritical crack growth, we do not consider them explicitly in this current study.

[4] Our goal in the present work has been to study the formation of fluid pressure-driven fractures in rock in the brittle regime by means of monitoring the temporal and spatial distribution of acoustic emission activity. We generated fluid pressure-driven fractures in samples of Darley Dale sandstone in a 400 MPa triaxial cell, and recorded the associated AE data sets. To enhance our interpretation, we also modeled the mechanical behavior of fluid pressure-driven fracturing in sandstone using a Particle Flow Code

0094-8276/04/2004GL019638

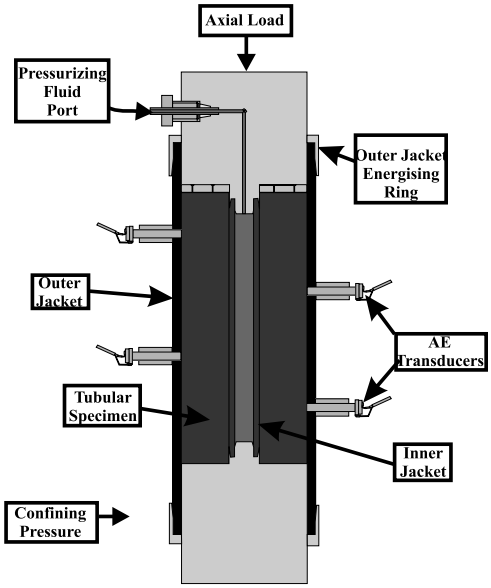

Figure 1. Internal sample assembly for pressure-driven fracture experiments.

(PFC), which, on the basis of input micro-parameters, defines the dynamics of fluid pressure-driven fractures from the macro-parameters measured in the laboratory. This modeling technique also provides the unique ability to produce acoustic emission, thereby enabling a direct quantitative comparison between AE recorded in the laboratory experiment to AE produced by the model.

2. Experimental Details

2.1. Sample Material

[5] Darley Dale sandstone is a poorly sorted, well-indurated felspathic sandstone from the north of England. The cementing material is predominantly silicious, and a modal analysis gives a composition of 69% quartz, 22% feldspar, 3% mica and 6% clay. The grain size ranges from 0.08 mm to 0.80 mm, with a mean grain diameter of 0.34 mm. The rock has a total porosity of approximately 13%.

2.2. Experimental Procedure

[6] Experiments were performed in a silicon oil-medium high-pressure triaxial deformation cell in the Mineral, Ice and Rock Physics Laboratory at University College London. The cell has a servo-controlled loading system, and servo-control of the pore fluid pressure. In addition, it incorporates a multi-transducer system for the measurement of changes in rock physical properties.

[7] Cylindrical rock samples (40 mm diameter $\times$ 100 mm long) were all cored from a single block of Darley Dale sandstone, and co-axially pre-drilled with an 8 mm hole to allow access for the internal pressurizing fluid. Samples were jacketed both internally and externally, with nitrile rubber jackets, as shown in Figure 1. The external jacket prevents the silicon oil confining fluid from penetrating the sample, and provides inserts for up to 12 measurement transducers. In these experiments, eight 3 mm piezoelectric acoustic emission transducers of 1 MHz resonant frequency were attached, and connected to a fast acoustic emission recording system (Spartan SP-3DL) via low-noise pre-amplifiers (40dB). Locations have been obtained by inverting arrival time data as a function of transducer position and sample geometry, adopting a velocity field of 3.5 km/s. Only those emissions that were recorded at a minimum of 4 transducers were used in the location process. The internal jacket allows the inner bore to be pressurized while preventing the pressurizing fluid from penetrating the sample. This is necessary because the sample material has a high permeability (about 0.3×10^{-12} m^2), and we need to pressurize slowly in order to study the detail of the fracture formation process.

[8] All experiments were performed under a constant confining pressure of 6–7 MPa. An axial load of 50 MPa was also applied to ensure sealing of the sample assembly. The internal pressure was then increased at constant rate of 1 MPa per minute until pressure driven fractures nucleated and subsequently propagated to the outer boundary of the sample. In order to address the problem of scale, we chose an external to internal diameter ratio of 5:1 for our samples. For the case of hydrostatic confining pressure, as used in our experiments, the general solutions for the stress distribution around a circular hole in an infinite plate reduces to the Lamé solutions for the stress around an infinitely thick-walled cylinder [*Jaeger and Cook*, 1979]. For our diameter ratio, the infinite solutions can be applied with only a 4% error.

3. Experimental Results

[9] We observe two distinct peaks of AE activity during fluid pressure-driven fracturing (Figure 2a). Although more

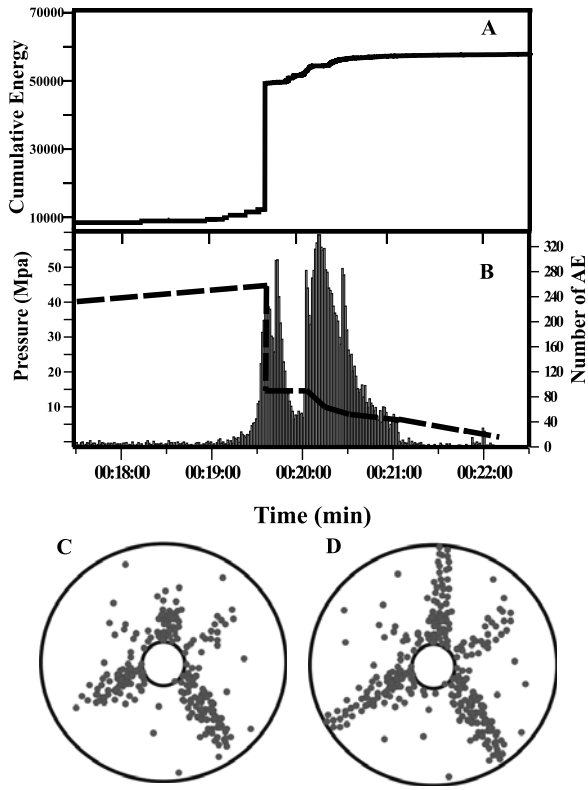

Figure 2. (a) Cumulative AE energy release, and (b) number of AE events and inner bore pressure, plotted against time for a pressure-driven fracture experiment; (c) locations of AE events up to the first AE peak, and (d) after the fractures had propagated to the sample boundary.

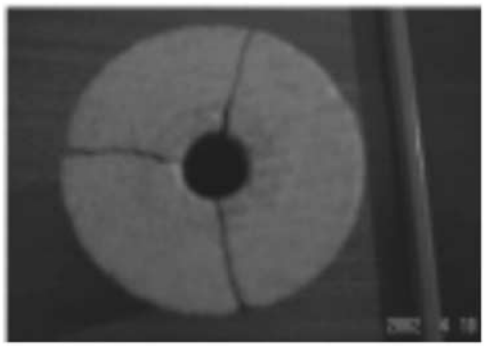

Figure 3. Post-test pressure driven fractures. 3 main fractures at 120° propagated to the edge of the sample.

AE events are generated in the second peak, the bulk of the energy release (Figure 2b) is clearly associated with the first peak. The time evolution of AE locations is shown in Figures 2c and 2d. Figure 2c shows the locations of events associated with the first peak in Figure 2a, while Figure 2d shows all located events up to the end of the experiment. The location data strongly support the conclusion that the first burst of activity, which includes the bulk of AE energy, corresponds to fracture initiation. Initiation occurs at a critical value of internal pressure (22–23 MPa) that is approximately three times the external confining pressure, and is associated with a significant drop in internal pressure. Fracture extension stabilises at this point due to a balance between the internal and external pressures, since the internal pressurizing fluid is prevented from penetrating the fractures by the internal jacket. Further application of internal pressure is therefore required to propagate the fractures to the outer boundary of the sample (Figure 2c), and this second phase of activity is accompanied by a much smaller drop in internal pressure (Figure 2a).

[10] From both AE locations and recovered samples (Figure 3) we observe initiation of three main fractures, and up to three subsidiary ones. However, only the three main fractures, which form at approximately 120°, propagate to the outer boundary. This geometry has shown good repeatability over the 10 experiments carried out.

4. The Model Particle Flow Code (PFC)

[11] A numerical model of the experiment was generated using the Particle Flow Code [*Itasca Consulting Group*, 1999]. With this technique, a competent rock is modeled as an assembly of circular particles joined by breakable bonds. Micro parameters (particle stiffness, bond strengths, particle packing, etc.) dictate the macro behavior of the material [*Potyondy and Cundall*, 2004]. The models are fully dynamic, and an explicit calculation scheme is used such that stored strain energy can be released from contacts when bonds break and simulated AE can propagate through the system [*Hazzard and Young*, 2002]. A PFC model of a 2D slice of the sample was created using 25,000 particles ranging in size from 0.08 to 0.8 mm, to replicate the grain size distribution of Darley Dale sandstone. Particle stiffnesses and bond strengths were assigned such that the model exhibited the same stiffness and tensile strength as Darley Dale sandstone. Inner and outer jackets were modeled by a layer of particles with stiffnesses 100 times lower than the rock particles (to simulate the compliant rubber sleeves). A confining pressure of 6.5 MPa was maintained by controlling the velocities of the outer sample particles. The inner bore was pressurized by applying a constant outward radial velocity to the inner jacket particles (Figure 4a). This approach was chosen because it allows us to reproduce the experiment up to the point of fracture initiation, which our experiments suggest is the most significant point in the process. During pressurization of the inner bore, sparse microcracking (bond breakage) commences around 17 MPa, as indicated by the onset of AE (Figure 4b). The AE rate increases as the inner pressure is increased, until coalescence of microcracks leads to the initiation of 5 to 6 macrofractures around 28 MPa (Figures 4b and 4c), in relatively good agreement with the experimental results. The slight discrepancy is considered to be due to the loss of one degree of freedom in using a 2D simulation. The model is useful to understand damage accumulation and fracture initiation, however, the model data during fracture propagation is not quantitatively meaningful. We nevertheless ran the model until fractures intersected the external boundary of the sample, as this can provide a qualitative comparison with the experimental fracture geometries. The geometry resulting from running the model in this way is shown in Figure 4d, where three main fractures, at approximately 120°, are seen to extend to the edge of the sample.

5. Discussion

[12] AE locations show that a set of 3 to 6 fractures originated at the wall of the internal bore at a critical internal

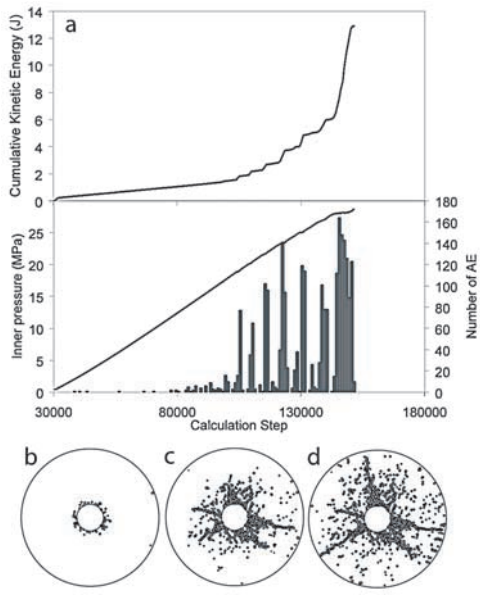

Figure 4. (a) Cumulative AE and inner bore pressure produced by the PFC model plotted against step number (equivalent to time). Locations of simulated AE events are shown for (b) the onset of microfacturing around 17 MPa, (c) the initiation of macrofactures around 28 MPa, and (d) the propagation of three macrofractures to the sample boundary.

pressure around three times that of the external confining pressure. Approximately 70% of the total AE energy is released during this initial phase of activity. Fracture initiation is associated with a significant drop in internal pressure, and further pressurization of the internal bore is then required to propagate the fractures to the external boundary. The propagation phase is associated with a large number of AE events, but with significantly less energy. Only three main fractures, at approximately 120° to each other, propagate to the sample boundary. This geometry is remarkably similar to the 120° three-armed rift zone geometry reported for oceanic island volcanoes, where vents and dense dyke swarms concentrate [*MacDonald*, 1972; *Carracedo*, 1994, 1999].

[13] Initiation of the macro-fractures is preceded by a precursory period of accelerating AE activity (Figure 2) that lasts approximately 45 seconds. It is well known that shear fracture of Darley Dale sandstone under triaxial compression is preceded by an extended period of precursory AE activity [e.g., *Meredith et al.*, 1990], since localized shear failure is achieved through the coalescence of many microcracks. By contrast, we would intuitively expect a much reduced level of precursory activity before pressure-driven tensile fracturing. This observation may help to explain the relatively short duration (hours to days) of seismic swarms recorded prior to the formation and/or propagation of fracture systems leading to eruption onset in volcanic areas [*Minakami*, 1974; *Hill*, 1977].

[14] The experiment was also simulated numerically by representing the material as an assembly of bonded particles. The numerical model quantitatively reproduces the most important features of the time and spatial distribution of AE observed in the laboratory experiments. Microcracking around the central bore started around 17 MPa, well before the peak pressure was reached. Importantly, the simulation reproduces the precursory phase of AE activity, with AE commencing when diffuse microcracks form around 17 MPa and accelerating to the point where 5 to 6 macrofractures initiate around 28 MPa. Finally, three main fractures propagate to the edge of the sample at approximately 120° to each other. This suggests that, for a relatively homogeneous rock in an axisymmetric stress field, the propagation of three evenly distributed radial fractures may represent the most efficient geometry for energy dissipation. Interestingly, this pattern is also ubiquitous in the cooling joints observed in columnar basalt flows.

[15] **Acknowledgments.** S.V. was funded by a Marie Curie Individual Fellowship (Contract n. FMBICT983260). N. Hughes is particularly thanked for his crucial support during laboratory experiments. O. Clint, S. Boon and J. Bowles are thanked for fruitful discussions and their support for the experimental work.

References

Carracedo, J. C. (1994), The Canary Islands: An example of structural control on the growth of large oceanic-island volcanoes, *J. Volcanol. Geotherm Res.*, *72*, 151–162.

Carracedo, J. C. (1999), Growth, structure, instability and collapseof Canarian volcanoes and comparisons with Hawaiian volcanoes, *J. Volcanol. Geotherm Res.*, *94*, 1–19.

Hanks, T. C. (1992), Small earthquakes, tectonic forces, *Science*, *256*, 1430–1432.

Hazzard, J. F., and R. P. Young (2002), Moment tensors and micromechanical models, *Tectonophysics*, *356*, 181–197.

Hill, D. (1977), A model for earthquake swarms, *J. Geophys. Res.*, *82*, 1347–1352.

Itasca Consulting Group (1999), *Particle Flow Code in 2 Dimensions*, version 2.0, Itasca Consult. Group, Inc., Minneapolis, Minn.

Jaeger, J. C., and N. G. W. Cook (1979), *Fundamentals of Rock Mechanics*, 3rd. ed., 593 pp., Chapman and Hall, New York.

Lister, J. R., and R. C. Kerr (1991), Fluid-mechanical models of crack propagation and their application to magma transport in dykes, *J. Geophys. Res.*, *96*, 10,049–10,077.

Lockner, D. A., J. D. Byerlee, P. V. Kuksenko, A. Ponomarev, and A. Sidorin (1991), Quasi-static fault growth and shear fracture energy in granite, *Nature*, *350*, 39–42.

MacDonald, G. A. (1972), *Volcanoes*, Prentice–Hall, Englewood Cliffs, N. J.

Meredith, P. G., I. G. Main, and C. Jones (1990), Temporal variations in seismicity during quasi-static and dynamic rock failure, *Tectonophysics*, *175*, 249–268.

Minakami, K. (1974), Prediction of volcanic eruptions, in *Physical Volcanology*, edited by L. Civetta et al., pp. 313–333, Elsevier Sci., New York.

Nur, A., and J. Walder (1992), Hydraulic pulses in the Earth's crust, in *Fault Mechanics and Transport Properties of Rocks*, *Int. Geophys. Ser.*, vol. 51, edited by B. Evans and T. F. Wong, pp. 461–473, Academic, San Diego, Calif.

Pollard, D. D. (1987), Elementary fracture mechanics applied to the structural interpretation of dykes, in *Mafic Dyke Swarms*, edited by H. C. Halls and W. H. Fahrig, *Geol. Assoc. Can. Spec. Pap.*, *34*, 5–24.

Potyondy, D., and P. Cundall (2004), A bonded particle model for rock, *Int. J. Rock Mech. Min. Sci.*, in press.

Rubin, A. M. (1993), Why geologists should avoid using 'fracture toughness' (at least for dykes), in *Physics and Chemistry of Dykes: Selected Papers Presented at the Third International Dyke Conference*, *Jerusalem/Israel/4-8 September 1995*, edited by G. Baer and A. Heimann, pp. 53–63, A. A. Balkema, Brookfield, Vt.

Secor, D. T., and D. D. Pollard (1975), On the stability of open hydrofractures in the Earth's crust, *Geophys. Res. Lett.*, *2*, 510–513.

Spence, D. A., and D. L. Turcotte (1985), Magma driven propagation of cracks, *J. Geophys. Res.*, *90*, 575–580.

Weertman, J. (1971), Theory of water-filled crevasses in glaciers applied to vertical magma transport beneath oceanic ridge, *J. Geophys. Res.*, *76*, 1171–1183.

Zang, A., F. C. Wagner, S. Stanchits, G. Dresen, R. Andresen, and A. Haidekker (1998), Source analysis of acoustic emissions in Aue granite cores under symmetric and asymmetric compressive loads, *Geophys. J. Int.*, *135*, 1113–1130.

P. G. Meredith, Mineral, Ice and Rock Physics Laboratory, Department of Earth Sciences, University College London, London WC1E 6BT, UK.

J. Hazzard, Lassonde Institute, Room 119, 170 College Street, University of Toronto, Toronto, Ontario, Canada M5S 3E3.

S. Vinciguerra, Osservatorio Vesuviano, Istituto Nazionale di Geofisica e Vulcanologia, I-80124 Naples, Italy. (vinciguerra@ov.ingv.it)